

FAST 3D MODELING OF BOREHOLE INDUCTION DATA IN DIPPING AND ANISOTROPIC FORMATIONS USING A NOVEL APPROXIMATION TECHNIQUE

Guo-zhong Gao, and Carlos Torres-Verdín
Department of Petroleum and Geosystems Engineering, the University of Texas at Austin

Sheng Fang
Baker Atlas, Houston, TX

ABSTRACT

Macroscopic electrical anisotropy of rock formations can substantially impact estimates of fluid saturation performed with borehole electromagnetic (EM) measurements. To date, accurate and expedient numerical simulation of the EM response of anisotropic and dipping formation remains an open challenge. The presence of a borehole and mud-filtrate invasion further complicates the possibility of an efficient numerical solution.

This paper introduces a novel 3D integral equation approximation to simulate EM borehole measurements. The approximation makes use of an integral equation formulation in which the Green's tensor is defined over a homogeneous and isotropic background. Moreover, the approximation makes explicit use of spatially smooth representations of the electric field internal to EM scatterers. It also considers the relatively large contribution due to the proximity of transmitters and receivers to rock formations immediately adjacent to the borehole wall. A simple vectorial representation of the internal electric field is used to properly describe changes in polarization due to conductivity anisotropy. For a prescribed degree of spatial smoothness, the vectorial representation of the internal field is adjusted using an optimal least-squares criterion. This strategy provides the EM coupling properties necessary to accurately simulate scattering in anisotropic media.

Several examples are described of the performance of the new scattering approximation when used in the simulation of multi-component induction tools. Tests of accuracy and computer efficiency are considered against 1D and 3D finite-difference solutions previously described in the context of dipping and anisotropic formations. An assessment of the new approximation is also performed to quantify the influence on accuracy of the number of discretization blocks used to describe the spatial smoothness of the internal electric field. Finally, a criterion is introduced to select the value of background conductivity in an optimal manner.

The accuracy and efficiency of the new approximation successfully compete with those of accurate finite-difference formulations. Numerical simulations involving more than 10^6 discretization cells usually require only several minutes per frequency and tool location on a Silicon Graphics workstation. Additional tests of accuracy of the new approximation technique are performed against alternative approximation techniques, such as Born, Extended Born, and Quasi-Linear. Results of this exercise indicate that the new approximation provides superior accuracy to that of standard approximations without much compromise on computer efficiency.

INTRODUCTION

Integral equations have been widely used to simulate EM scattering, including applications in geophysical prospecting and antenna design. Hohmann (1971) first discussed the application of integral equations for the simulation of two-dimensional (2D) subsurface geophysical problems. Since then, a number of applications and developments have been reported that include 3D EM scattering in the presence of complex geometrical structures (e.g. Hohmann, 1975, and 1983, Wannamaker, 1983, Xiong, 1992, Gao, 2002, and Fang et al., 2003, among others).

Solution of EM scattering by integral equations includes two serial steps. First, the spatial distribution of electric fields within scatterers is computed via a discretization scheme. Second, the internal scattering currents are "propagated" to receiver locations. It is often necessary to discretize the scatterers into a large number of cells depending on (a) frequency, (b) conductivity contrast, (c) size of the scatterers, and (d) proximity of the source and/or the receiver to the scatterers. This discretization gives rise to a full complex linear system of equations whose solution yields the spatial distribution of internal electric fields. Requirements of computer memory storage increase quadratically with an increase in the number of discretization cells. Moreover, the need to solve a large, full, and complex linear system of equations

places significant constraints on the applicability of 3D integral equation methods.

There are several numerical strategies used to overcome the difficulties associated with integral equation formulations of EM scattering. Fang *et al.* (2003) recently reported one such strategy. Their simulation approach makes explicit use of the symmetry properties of Toeplitz matrices. Fang *et al.*'s (2003) algorithm also applies a suitable combination of BiCGSTAB(1) (Bi-Conjugate Gradient STABILized (1)) (Gerard and Diederik, 1993) and the FFT (Fast Fourier Transform) to iteratively solve the linear system of equations. The latter method is a natural extension of the widely used CG-FFT (Conjugate Gradient-Fast Fourier Transform) strategy (Catedra *et al.*, 1995) to compute EM fields. Despite these significant improvements, integral equation methods are still impractical for routine use in the interpretation of borehole EM data. An alternative approach is to develop an approximate solution. Several approximations to the integral equation formulation have been proposed in the past. These include Born (1933), Extended Born (Habashy *et al.*, 1993; and Torres-Verdin and Habashy, 1994), and Quasi-Linear (Zhadnov and Fang, 1996). However, to date none of these approximations have been adapted to approach 3D EM scattering in the presence of anisotropic media.

Very recently, a novel approximation technique was introduced that has the ability to accurately and efficiently model borehole EM scattering in the presence of anisotropic rock formations (Gao *et al.* 2003). This paper describes further developments performed in the implementation, testing, and benchmarking of Gao *et al.*'s (2003) novel integral equation approximation. The approximation attempts to synthesize the spatial variability of the secondary electric currents within a scatterer in two manners. First, a multiplicative term is introduced to "capture" the variability of the secondary electric currents due to the close proximity of the EM source to the scatterer. A second multiplicative term is used to synthesize phase and polarization variations of the secondary electric currents due to spatial variations in electrical conductivity, including those due to anisotropy. It is shown that for borehole logging applications the latter multiplicative term is spatially smoother than the first term and hence can be described with fewer discretization blocks. Moreover, the accuracy of the proposed approximation depends on both the choice of the background model and the spatial distribution and number of discretization blocks.

This paper is organized as follows: First the integral equation method is introduced together with the theory and physical intuition behind the new approximation. Subsequently, technical details are provided concerning the choice of a background conductivity value. A section is also included to assess the influence of the spatial block discretization constructed within EM scatterers. Simulation examples are used to compare the accuracy of the new approximation against alternative integral equation approximations, i.e. Born, and Extended Born. Finally, several examples are provided to illustrate the performance of the new approximation in the presence of finite-size boreholes, mud-filtrate invasion, and conductivity anisotropy of rock formations. These examples assume EM sources and receivers in the form of multi-component borehole logging tools.

THEORY OF INTEGRAL EQUATION MODELING

Assume an EM source that exhibits a time harmonic dependence of the type $e^{-i\omega t}$. The magnetic permeability of the medium equals that of free space, \mathbf{m}_0 . Thus, the integral equation for electric and magnetic fields is in general given by (Hohmann, 1975)

$$\mathbf{E}(\mathbf{r}) = \mathbf{E}_b(\mathbf{r}) + \int_t \overline{\overline{G}}(\mathbf{r}, \mathbf{r}_0) \cdot \Delta \overline{\overline{\mathbf{S}}}(\mathbf{r}_0) \cdot \mathbf{E}(\mathbf{r}_0) d\mathbf{r}_0, \quad (1)$$

and

$$\mathbf{H}(\mathbf{r}) = \mathbf{H}_b(\mathbf{r}) + \int_t \overline{\overline{G}}^h(\mathbf{r}, \mathbf{r}_0) \cdot \Delta \overline{\overline{\mathbf{S}}}(\mathbf{r}_0) \cdot \mathbf{E}(\mathbf{r}_0) d\mathbf{r}_0, \quad (2)$$

where $\mathbf{E}(\mathbf{r})$ and $\mathbf{H}(\mathbf{r})$ are the electric and magnetic field vectors, respectively, at the measurement location \mathbf{r} . $\mathbf{E}_b(\mathbf{r})$ and $\mathbf{H}_b(\mathbf{r})$ are the electric and magnetic field vectors, respectively, associated with a homogeneous, unbounded, and isotropic background medium of dielectric constant \mathbf{e}_{rb} and conductivity \mathbf{s}'_b . Accordingly, the background complex conductivity is given by $\mathbf{s}_b = \mathbf{s}'_b - i\omega \mathbf{e}_{rb} \mathbf{e}_0$, and the wavenumber, k_b , of the background medium is given by $k_b^2 = i\omega \mathbf{m}_0 \mathbf{s}_b = \omega^2 \mathbf{m}_0 \mathbf{e}_0 \mathbf{e}_{rb} + i\omega \mathbf{m}_0 \mathbf{s}'_b$. At low frequencies, the expression for the background wavenumber simplifies to $k_b^2 = i\omega \mathbf{m}_0 \mathbf{s}'_b$.

The electric Green's tensor included in equations (1) and (2) can be expressed in closed form as

$$\bar{\bar{G}}^e(\mathbf{r}, \mathbf{r}_0) = (i\omega\mathbf{m}_0 \bar{\bar{I}} + \frac{1}{\mathbf{s}_b} \nabla \nabla) g(\mathbf{r}, \mathbf{r}_0), \quad (3)$$

where the scalar function $g(\mathbf{r}, \mathbf{r}_0)$ satisfies the wave equation

$$\nabla^2 g(\mathbf{r}, \mathbf{r}_0) + k_b^2 g(\mathbf{r}, \mathbf{r}_0) = -\mathbf{d}(\mathbf{r} - \mathbf{r}_0), \quad (4)$$

and whose solution can be explicitly written as

$$g(\mathbf{r}, \mathbf{r}_0) = \frac{e^{ik_b|\mathbf{r}-\mathbf{r}_0|}}{4\pi|\mathbf{r}-\mathbf{r}_0|} = \frac{e^{ik_b R}}{4\pi R}. \quad (5)$$

The magnetic Green's tensor is related to the electric Green's tensor through the expression

$$\bar{\bar{G}}^h(\mathbf{r}, \mathbf{r}_0) = \frac{1}{i\omega\mathbf{m}_0} \nabla \times \bar{\bar{G}}^e(\mathbf{r}, \mathbf{r}_0). \quad (6)$$

Finally, the tensor

$$\bar{\bar{\Delta}}\mathbf{s} = \bar{\bar{\mathbf{s}}} - \mathbf{s}_b \bar{\bar{I}} = \bar{\bar{\Delta}}\mathbf{s}' - i\omega\mathbf{m}_0 \Delta\mathbf{e}_r \mathbf{e}_0 \bar{\bar{I}}$$

is the complex conductivity contrast within scatterers, with $\Delta\mathbf{e}_r = \mathbf{e}_r - \mathbf{e}_{rb}$, $\bar{\bar{\Delta}}\mathbf{s}' = \bar{\bar{\mathbf{s}}}' - \mathbf{s}_b' \bar{\bar{I}}$, and $\bar{\bar{I}}$ a unity tensor.

Equations (1) and (2) are Fredholm integral equations of the second kind. A solution of these equations can be obtained using the method of moments (MoM). Traditional implementations of the MoM yield a full matrix equation, which normally involves the following difficulties for large-scale numerical simulation problems: (a) matrix filling time is substantial; (b) very large memory storage requirements; and (c) time-consuming solution of the complex linear system of equations. For large 3D scatterers, often the solution to EM scattering cannot be approached with a naïve implementation of the MoM. For instance, in a modeling example involving 1 million discretization cells, 0.2 CPU seconds are needed to compute 10,000 entries (each entry is a 3 by 3 tensor) of the linear-system matrix. Table No. 1 summarizes two of the most significant computer requirements associated with this hypothetical example. Quite obviously, such requirements place rather impractical constraints to most of today's computer platforms.

Matrix filling time	231.48 days
Memory storage (single complex precision)	33,527 Gigabytes

Table 1. Matrix filling time and computer storage associated with the assumption of 1 million discretization cells, and 0.2 CPU seconds needed to compute 10,000 entries (each entry is a 3 by 3 tensor) of the MoM's linear-system matrix.

Very recently, a method has been reported (Fang *et al.*, 2003) to approach the same problem. This method makes use of BiCGSTAB(1) and the FFT to take advantage of the symmetry properties of Toeplitz matrices arising in the solution of integral equations with uniform spatial grids. The properties of a Toeplitz matrix resemble those of a sparse matrix, whereupon only a relatively small portion of the matrix is required for matrix filling time and memory storage. However, this solution is still time consuming for calculating a borehole logging profile as the computation time ranges from 20 minutes to one hour for a single source location.

A NEW EM SCATTERING APPROXIMATION

The EM scattering approximation reported in this paper is based on a new formulation of the integral equation (1). In so doing, the total electric field vector within each discretization cell is expressed as the product of the magnitude of the background field and a polarization vector, namely,

$$\mathbf{E}(\mathbf{r}) = \mathbf{d}(\mathbf{r}) e_b(\mathbf{r}), \quad (7)$$

where

$$e_b(\mathbf{r}) = (\mathbf{E}_b^*(\mathbf{r}) \cdot \mathbf{E}_b(\mathbf{r}))^{1/2}, \quad (8)$$

and

$$\mathbf{d}(\mathbf{r}) = \begin{pmatrix} d_x \\ d_y \\ d_z \end{pmatrix} (\mathbf{r}). \quad (9)$$

The scalar factor of the product in equation (7) is used to synthesize the relative spatial changes in magnitude of the electric field, whereas the vector factor in the same equation is used to synthesize relative spatial changes in the polarization, phase, and to a less extent, of the amplitude of the electric field.

Equation (1) then becomes

$$e_b(\mathbf{r})\mathbf{d}(\mathbf{r}) = \mathbf{E}_b(\mathbf{r}) + \int_t \overline{\overline{G}}(\mathbf{r}, \mathbf{r}_0) \cdot \overline{\overline{\Delta\mathbf{S}}}(\mathbf{r}_0) \cdot e_b(\mathbf{r}_0)\mathbf{d}(\mathbf{r}_0) d\mathbf{r}_0 \cdot (10)$$

The new approximation stems directly from this last integral equation. In the above expression, e_b embodies relative changes in the magnitude of the internal electric field due to the proximity of the EM source. The larger the distance from the EM source to the scatterer, the less significant the spatial changes of e_b within the scatterer. In the far field, one would expect e_b to be spatially constant within the scatterer.

The spatial smoothness criterion necessary to accurately describe vector \mathbf{d} depends, to some extent, on the proximity of the EM receiver to the scatterer. Equation (1) shows that the simulation of EM scattering at the receiver location is obtained by “propagating” the internal scattering electrical currents to the EM receiver location. In this case, the “propagator” is given by the electric Green’s tensor,

$$\overline{\overline{G}}(\mathbf{r}_R, \mathbf{r}_0),$$

where \mathbf{r}_R is the EM receiver’s location and \mathbf{r}_0 is a point within the scatterer. The effect of the “propagator” can also be thought of as an operation wherein the scattering current,

$$\overline{\overline{\Delta\mathbf{S}}}(\mathbf{r}_0) \cdot \mathbf{E}(\mathbf{r}_0),$$

is spatially low-pass filtered (i.e. it is smoothed in space) to provide the value of the electric field at the EM receiver’s location. For a constant frequency, such a smoothing operation becomes more pronounced as the receiver recedes away from the scatterer. In the case of a fixed transmitter-receiver configuration, such as in borehole induction logging, the “propagator” itself provides a precise measure of the degree of smoothness necessary to compute accurate solutions of the scattered EM field at the receiver location. In other words, even though scattering currents may exhibit large spatial variations within the scatterer, these spatial variations are effectively smoothed when “propagated” to the receiver location. Because of this important remark, it is only necessary to calculate scattering currents with accuracies consistent with those of the spatial smoothing properties of the “propagator.”

The criterion adopted in this paper to control the degree of spatial smoothness of the internal electric field consists of discretizing the scatterer into a collection of blocks, each block being composed of several cells. This procedure assumes that within each block the \mathbf{d} vector is constant, whereas the term e_b is assumed variable within a block but constant within a

cell. Because of the choice of a uniform spatial discretization grid, all cells exhibit the same shape and size. The spatial distribution and size of blocks, however, can be chosen in a more flexible manner. It is only required that blocks be built to conform to cell boundaries. Finally, a least-squares minimization approach is used to solve for the \mathbf{d} vector associated with a given block via equation (1). Such a procedure gives rise to a reduced linear system of equations for the unknown vector \mathbf{d} within each discretization block, thereby substantially decreasing memory storage and CPU time requirements. Additional savings in computer storage and CPU execution time are obtained with the use of uniform spatial discretization scheme and a Toeplitz matrix formulation. When using uniform discretization grids, a Toeplitz matrix is constructed for each discretization block. Matrix vector multiplications are further accelerated using the FFT (Fast Fourier Transform).

ON THE CHOICE OF A VALUE OF BACKGROUND ELECTRICAL CONDUCTIVITY

As described above, the new approximation involves two conformal spatial discretization volumes. The first one is constructed using fine cells to describe the spatial variability of the scalar term e_b . In turn, the specific value of e_b assigned to a given cell depends on the assumed background model. This suggests the possibility of selecting the value of background conductivity to provide the largest possible accuracy within the practical limits of the approximation.

A criterion to choose the background model is to make a compromise between the contribution of small and large conductivity values in the formation model, or else to minimize the difference between the minimum and maximum formation conductivity values using some weighted metric. Extensive numerical experiments suggested that the geometrical average of the minimum and maximum formation conductivity values provided optimal results for the examples considered in this paper. This geometrical average is given by

$$s_b = \sqrt{s_{\min} \cdot s_{\max}} \cdot (11)$$

The above result is also suggested by studies in the theory of effective media involving the electrical conductivity of two-dimensional composites, a subject originally considered by A.M. Dykhne (1970). Using Dykhne’s theory, it can be shown that a symmetric mixture of two components exhibits an effective conductivity given by the geometrical average of the

conductivities of the constituent materials. Alternative procedures could exist to choose an optimal background conductivity value. These could include weighted averages of the conductivity distribution, where the weights would be determined by (a) proximity to the source(s), (b) proximity to the receiver(s), and (c) block volume.

Quite obviously, the choice of a background conductivity value other than that of the borehole conductivity causes the borehole itself to become part of the anomalous conductivity region. Because of this, memory and CPU requirements increase when computing the internal electric field. Despite these difficulties, numerical experiments show that the choice of background conductivity described by equation (11) does not substantially compromise the efficiency of the simulation algorithm. The small sacrifice in computer efficiency is drastically outweighed by the gain in numerical accuracy. Moreover, the implementation of the integral equation algorithm described in this paper makes use of 3D FFTs that require of a uniform and spatially continuous discretization grid for their implementation. This includes the borehole region, whereupon the algorithmic implementation considered in this paper naturally lends itself to a choice of background conductivity value other than that of the borehole.

SENSITIVITY TO THE CHOICE OF SPATIAL DISCRETIZATION

As emphasized above, there are two levels of spatial discretization involved in the computation of the integral equation approximation described in this paper. A fine cell structure is first constructed to describe the spatial variations within the scatterer of the scalar factor e_b contained in eq. (10). The relative spatial variations of this factor are primarily controlled by the proximity of the EM source to the scatterers. On the other hand, a relatively larger conformal block structure is constructed to describe the spatial variations of vector \mathbf{d} . A given block in the discretization scheme of vector \mathbf{d} is composed of several cells used for the spatial discretization of the scalar factor e_b . The specific choice of block and cell structure may have a significant influence on the performance of the approximation.

The strategy chosen in this paper to construct block structures is one in which small blocks are placed in close proximity to the borehole, the transmitter(s), and the receiver(s). Relatively larger blocks are used to discretize the remaining spatial regions in the

scattering rock formations. This choice is consistent with the expected spatial distribution of scattering currents.

Figure 1 shows the model used in this paper to study the effect of various block structures on the accuracy of the newly developed scattering approximation. Simulation results are also intended to assess the accuracy and efficiency of the approximation in the presence of various rock formation properties, various dip angles, presence of a borehole, and presence of mud-filtrate invasion. This model was adapted from an example proposed by Wang and Fang (2001). It consists of 5 horizontal layers in which the top and bottom layers are isotropic and exhibit an electrical resistivity of 50 $\Omega\cdot\text{m}$. The third layer is a 50 $\Omega\cdot\text{m}$ isotropic layer of thickness equal to 12.0 ft. Finally, the second and fourth layers are anisotropic with a horizontal resistivity of 3 $\Omega\cdot\text{m}$ and a vertical resistivity of 15 $\Omega\cdot\text{m}$. Thickness of these two layers are 2.0 ft and 10.0 ft, respectively. Mud-filtrate invasion may also be present within these last two layers, with an invasion length equal to 36 in, and with the resistivity in the invaded zone equal to 3 $\Omega\cdot\text{m}$. The borehole has a diameter of 8.0 in. and a resistivity of 1 $\Omega\cdot\text{m}$.

Simulation results are computed for dip angles of 0 and 60 degrees for two cases of rock formation model: First, the formation is assumed to exhibit no invasion and no borehole, i.e. to consist of a 1D stack of layers. A second model does assume a rock formation with borehole and invasion. Invasion and borehole parameters for this model are as described in the preceding paragraph. We compare simulation results with those obtained using a 1D code (identified as “**1D**” in the figures) and the 3D finite difference simulation algorithm (identified as “**3D FDM**” in the figures) written by Wang and Fang (2001). In the descriptions and figures below, the identifier “**3D IE Appr.**” is used to designate simulation results obtained with the new approximation developed in this paper.

Figure 2 shows the borehole induction tool configuration assumed in the numerical simulations. It consists of one transmitter and two receivers moving in tandem along the borehole axis. Transmitter and receivers can be oriented in either of the x, y, and z directions. The spacing between the transmitter and the first receiver is 1.2m (L_1), whereas the spacing between the transmitter and the second receiver is 1.9m (L_2). It is further assumed that the tool measurement is a combination of the response

measured by the first magnetic receiver (H_1) and the second magnetic receiver (H_2), given by the formula

$$H = H_2 - \frac{L_1^3}{L_2^3} H_1 \cdot \quad (12)$$

Moreover, for the sake of conciseness but without sacrifice of generality, numerical simulations reported in this paper consider only the imaginary component of the variable H in equation (12). The real component of the same variable approaches zero at low frequencies (of the order of 25 KHz) and becomes approximately equal to its imaginary counterpart at high frequencies (of the order of 250 KHz).

In this section, attention is focused to a model with borehole and invasion, and the assumption is made of a borehole dip angle of 60° ; the operating frequency is 220KHz. Figure 3 describes the simulated H_{zz} field component, i.e. the vertical magnetic field component due to vertical magnetic source. This figure describes simulation results obtained using 8, 216, 1000, and 2400 discretization blocks, together with the corresponding results obtained with a 3D finite-difference code. In all of the above cases the number of discretization cells is 640,000. Figures 4 and 5 show the H_{xx} and H_{yy} components simulated for the same formation model, respectively. These figures suggest that 1000 discretization blocks already elicit accuracies similar to that of the 3D finite-difference code. Usage of 2400 blocks only provides a minor improvement over that of 1000 blocks. The same figures indicate that usage of only 8 blocks already produces the basic behavioral features of the magnetic field components H_{xx} , H_{yy} , and H_{zz} , thereby lending credence to the validity of the new approximation.

ASSESSMENT OF ACCURACY WITH RESPECT TO ALTERNATIVE APPROXIMATION TECHNIQUES

In the past, several types of integral equation approximations have been developed to approach large-scale EM simulation problems. These include Born (Born, 1933), Extended Born (Habashy, 1993; Torres-Verdin and Habashy, 1994), and quasi-linear (Zhadnov and Fang, 1996). The objective of this section is to assess the accuracy and efficiency of the new integral equation approximation in comparison with Born and extended Born approximations. The reader is referred to Gao *et al.* (2003) for a similar comparison with the quasi-linear approximation of Zhadnov and Fang (1996).

The formation model considered for this study is the same one used in the previous section. Simulation results are identified as follows: the label “**Born**” is used to designate simulations obtained with the first-order Born approximation, and the label “**ExBorn**” is used to designate results obtained with the Extended Born approximation. Figures 6 through 8 show the comparisons between simulation results for the three approximations for the H_{zz} ; H_{xx} ; and H_{yy} field components, respectively. Simulation results summarized in these figures indicate a superior performance of the new approximation with respect to the Born and extended Born approximations.

NUMERICAL EXAMPLES

Additional rock formation models and probing frequencies have been considered to further assess the accuracy and efficiency of the new approximation. These include: (a) a 1D formation that exhibits no borehole and no invasion, with a well dipping at an angle of 0° and 60° (the source direction dips at an angle of 0° and 60° with respect to the formation’s horizontal layering plane), (b) a 3D formation with borehole and invasion, with a well dipping at an angle of 0° and 60° (the borehole axis dips at angles of 0° and 60° with respect to the formation’s horizontal layering plane). The probing frequencies considered in the simulations are 20 KHz and 220 KHz. All of the examples considered in this section assume a multi-component induction tool for borehole logging.

The spatial discretization grid constructed for the simulations reported in this paper consists of 80 cells in the x direction, 80 cells in the y direction, and 100 cells in the z-direction. Cell sizes are kept uniform and equal to 0.1 m. In total, 2400 blocks are used for the discretization of the models considered in this paper. Figures 9 through 10 show simulation results (H_{zz} , H_{xx} , and H_{yy}) obtained with the new approximation assuming a 1D rock formation and a borehole dip angle of 0° . Simulation results for two frequencies (20 KHz and 220 KHz) are compared with those obtained with the 1D code. It is remarked that H_{xx} and H_{yy} remain identical when simulated along vertical wells and hence only one figure is shown here. Likewise, it is found that H_{zz} remains identical to the H_{zz} field component simulated for the case of an isotropic formation of conductivity equal to that of the horizontal conductivity. This result is customarily referred to as the “paradox of anisotropy” in induction log interpretation (Gianzero, 1999).

Figures 11 through 13 show simulation results (H_{zz} , H_{xx} , and H_{yy}) obtained with the new approximation assuming a 1D rock formation and a borehole dipping

at an angle of 60° . Simulation results for two frequencies (20 KHz and 220 KHz) are compared to those obtained with the 1D code. Figures 9 and 11 indicate a substantial sensitivity of H_{zz} to the presence of a dip angle. Similarly, a comparison of Figures 10 and 12 indicates a substantial sensitivity of H_{xx} to the presence of a dip angle. Yet greater effects due to the presence of a dip angle can be observed by comparing the simulated H_{yy} components.

Figures 14 and 15 show simulation results (H_{zz} , H_{xx} , and H_{yy}) obtained with the new approximation assuming a 3D rock formation (including both a borehole and invasion) but no dip angle. Simulation results for two frequencies (20 KHz and 220 KHz) are compared against those obtained with the 3D FDM code. The influence of a borehole and invasion can be clearly observed on the behavior of the simulated magnetic field components H_{zz} and H_{xx} .

Figures 16 through 18 show simulation results (H_{zz} , H_{xx} , and H_{yy}) obtained with the new approximation assuming a 3D rock formation (including both a borehole and invasion) and a dip angle of 60° . Simulation results for two frequencies (20 KHz and 220 KHz) are compared against those obtained with the 3D FDM code. A comparison of Figures 11 and 16 provides evidence of the sensitivity of the simulated magnetic field components H_{zz} and H_{xx} to the presence of both a borehole and invasion. By contrast, H_{xx} shows almost no sensitivity to the presence of a borehole and/or invasion.

The above simulation exercises consistently show that the newly developed approximation yields accurate results in the presence of complex 3D anisotropy models for the two probing frequencies considered in this paper (20 KHz and 220 KHz). Simulation of EM fields for one single borehole profile location entailed approximately 3-4 minutes on a 900MHz Sun workstation. By contrast, depending on the spatial discretization grid, it takes anywhere from 20 minutes to 1 hour of CPU time to simulate one EM borehole profiling location via a full-wave integral equation code developed by Fang *et al.*, 2003. The latter integral equation code was developed using similar algorithmic strategies to those used in the development of the new integral equation approximation.

CONCLUSIONS

This paper describes a new EM scattering approximation intended to substantially reduce computation times in the presence of complex 3D anisotropic formations. The approximation makes use

of a simple scalar-vectorial product to synthesize the smoothness properties of EM scattering currents. Additional computer efficiency for the approximation is achieved with the use of uniform discretization grids. Numerical simulations and comparisons against 1D and 3D finite-difference codes indicate that the new approximation remains accurate within the frequency range of borehole induction tools.

Numerical experiments indicate that the accuracy of new approximation depends on the choice of both the background conductivity value and the spatial block structure used for discretization. A criterion was described in this paper to select an optimal background conductivity value. Likewise, it was shown that only a relatively small number of spatial discretization blocks are needed to obtain accurate solutions of the EM fields measured at receiver locations.

Future work is envisioned for the construction of an optimal spatial block structure in an iterative manner. Such a procedure will commence with a sparse block structure that will be iteratively refined until no further improvement is observed in the EM fields computed at the receiver locations.

ACKNOWLEDGEMENTS

We are obliged to Dr. Tsili Wang, of Baker Atlas, for many useful discussions and for providing finite-difference simulation results for some of the test model examples described in this paper. The work reported in this paper was supported by UT Austin's Research Consortium on Formation Evaluation, jointly sponsored by Baker Atlas, Halliburton, Schlumberger, and Anadarko Petroleum Corporation. A note of gratitude goes to Baker Atlas for supporting summer internships for Guo-zhong Gao during 2001 and 2002. Part of the work reported in this paper was performed during these two summer internships.

NOMENCLATURE

s'	Ohmic conductivity.
ϵ_0	electrical permittivity of free space.
ϵ_r	dielectric constant.
μ_0	magnetic permeability of free space.
ω	angular frequency ($2\pi f$).
i	$=\sqrt{-1}$.
t	time.
$e^{-i\omega t}$	time convention.

$$\mathbf{s} = \mathbf{s}' - i\omega\mathbf{e}_r\mathbf{e}_0.$$

$\mathbf{r} = (x, y, z)$ Cartesian coordinates, equal to $x\hat{\mathbf{x}} + y\hat{\mathbf{y}} + z\hat{\mathbf{z}}$.

* superscript, denotes conjugate transpose.

= denotes a 3x3 tensor.

H_{xx} = magnetic field generated in x-direction by a x-directed source (the second x represents the source direction).

REFERENCES

- Born, M., 1933, Optics: Springer-Verlag, New York.
- Catedra, M.F., Torres, R.P., Basterrechea, J., and Gago, E., 1995, The CG-FFT method: Application of signal processing techniques to electromagnetics. Boston: Artech House.
- Fang, S., Gao, G-Z., and Torres-Verdín, C., 2003, Three-dimensional electromagnetic anisotropy modeling using integral equations, 3DEM III workshop, February 2003, Adelaide, Australia.
- Gao, G-Z., Fang, S. and Torres-Verdín, C., 2003, A New Approximation for 3D Electromagnetic Scattering in the Presence of Anisotropic Conductive Media, 3DEM III Workshop, February 2003, Adelaide, Australia
- Gao, G-Z., Torres-Verdín, C., Habashy, T. M, and Fang, S., 2002, Approximations to electromagnetic scattering based on natural preconditioners of the method-of-moments' stiffness matrix: applications to the probing of subsurface rock formations, presented at 2002 IEEE AP-S Internat. Symp. URSI Radio Science Meeting, San Antonio, TX, June 16-21.
- Gerard, L.G. Sleijpen and Diederik R. Fokkema, 1993, BiCGSTAB(l) for Linear Equations Involving Unsymmetric Matrices with Complex Spectrum, Electronic Transactions on Numerical Analysis, Vol. 1, pp.11-32.
- Gianzero, S., 1999, The paradox of anisotropy revisited, The Log Analyst, Vol. 40, No. 6, P.485-491
- Habashy, T.M., Groom, R.W. and Spies, B., 1993, Beyond the Born and Rytov approximations: A nonlinear approach to electromagnetic scattering, J. Geophys. Res., 98, 1759-1775.
- Hohmann, G.W., 1975, Three-dimensional induced polarization and electromagnetic modeling: Geophysics, Vol.40, No.2, pp. 309-324.
- Hohmann, G.W., 1983, Three-dimensional EM modelling, Geophys. Surv., 6, 27-53.
- Klein, J.D., Martin, P.R., and Allen, D.F., 1997, the petrophysics of electrically anisotropic reservoirs: The Log Analyst, May-June.
- Moran, J.H. and Gianzero, S., 1979, Effects of formation anisotropy on resistivity-logging measurements: Geophysics, Vol. 44, No. 7, P.1266-1286.
- Torres-Verdín, C. and Habashy, T.M., 2001, Rapid Numerical Simulation of Axisymmetric Single-well Induction Data using the Extended Born Approximation, Radio Science, Vol. 36, No. 6.
- Torres-Verdín, C. and Habashy, T.M., 1994, Rapid 2.5-dimensional forward modeling and inversion via a new nonlinear scattering approximation, Radio Science, Vol. 29, No. 4, P1051-1079.
- Wang T. and Fang S., 2001, 3-D electromagnetic anisotropy modeling using finite differences, Geophysics Vol. 66, No.5 P. 1386-1398.
- Wannamaker, P.E., Hohmann, G.W., SanFilipo, W.A., 1983, Electromagnetic modelling of three-dimensional bodies in layered earths using integral equations, Geophysics, Vol. 49, No. 1, pp. 60-74.
- Xiong, Z., 1992, Electromagnetic modeling of 3-D structures by the method of system iteration using integral equations: Geophysics, Vol. 57, No. 12, P.1556-1561.
- Zhdanov M. S. and Fang S., 1996, Quasi-linear approximation in 3-D electromagnetic modeling: Geophysics, Vol. 61, No. 3, P.646-665.

ABOUT THE AUTHORS

Guo-zhong Gao is currently a Ph.D candidate in the Department of Petroleum and Geosystems of The University of Texas at Austin. He obtained his Bachelor's degree and Master's degree from Southwest Petroleum Institute (China) and the University of Petroleum in Beijing in 1996 and 2000, respectively, all in Applied Geophysics. His current research interests include electromagnetic geophysics, numerical simulation, inverse scattering, and formation evaluation. Email: ggao@pe.utexas.edu.

Carlos Torres-Verdín received a Ph.D. in Engineering Geoscience from the University of California, Berkeley, in 1991. During 1991-1997, he held the position of Research Scientist with

Schlumberger-Doll Research. From 1997-1999, he was Reservoir Specialist and Technology Champion with YPF (Buenos Aires, Argentina). Since 1999, he is an Assistant Professor with the Department of Petroleum and Geosystems Engineering of The University of Texas at Austin, where he conducts research in formation evaluation and integrated reservoir characterization. He has served as Guest Editor for Radio Science, and is currently a member of the Editorial Board of the Journal of Electromagnetic Waves and Applications, and an associate editor for Petrophysics (SPWLA) and the SPE Journal. Email: cverdin@uts.cc.utexas.edu

Sheng Fang is currently a senior scientist and has been working on well logging applications with Baker Atlas since 1998. He received his BS (1984) and MS (1989) degrees in applied geophysics from China University of Geosciences (CUG) and his PhD (1998) degree in geophysics from the University of Utah (UU). His main research interests are in numerical simulation, practical inversion, and in developing data processing and interpretation techniques for different logging tools including resistivity, nuclear magnetic resonance (NMR), and pulse neutron capture (PNC) measurements. Email: sheng.fang@bakeratlas.com.

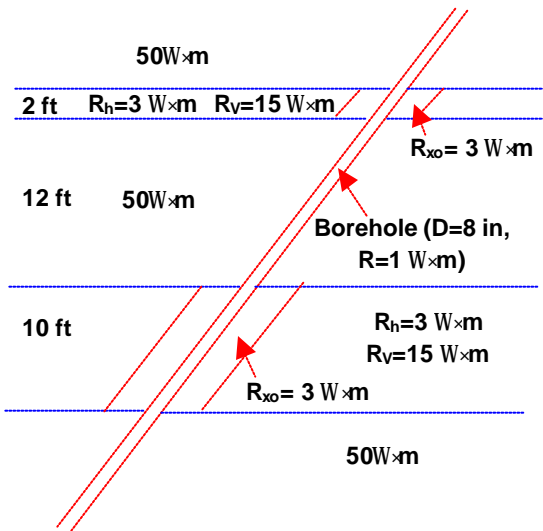


Figure 1. Graphical description of the generic 5-layer electrical conductivity model used in this paper to assess the accuracy and efficiency of the new integral equation approximation.

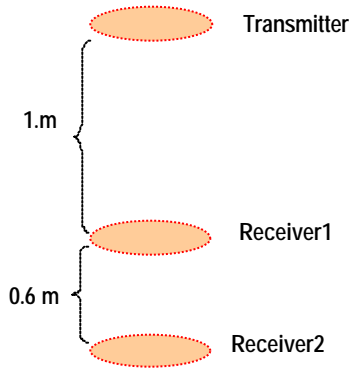


Figure 2. Assumed double receiver, single transmitter tool configuration for borehole induction logging (not to scale). In general, the transmitter and receivers may be oriented in x, y, and z directions.

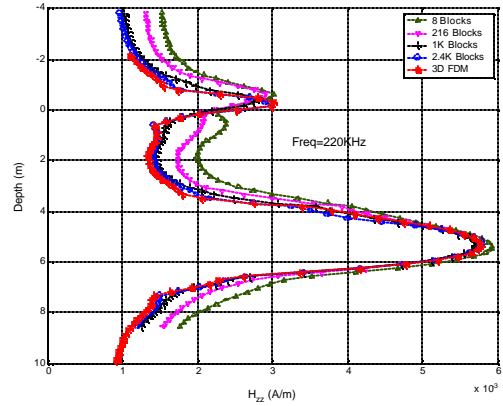


Figure 3. Assessment of the accuracy of the integral equation approximation of H_{zz} (imaginary part) for a given number of spatial discretization blocks. The formation dips at an angle of 60° and is modeled in the presence of both a borehole and mud-filtrate invasion. Simulation results are shown for a probing frequency of 220 KHz.

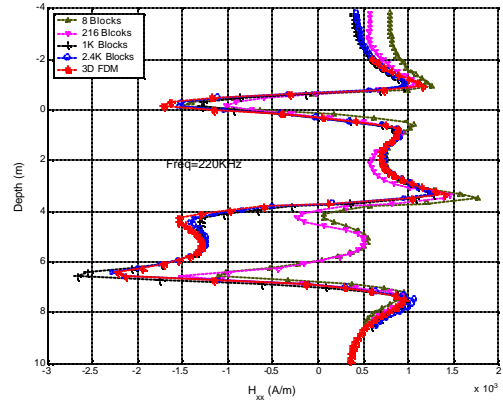


Figure 4. Assessment of the accuracy of the integral equation approximation of H_{xx} (imaginary part) for a given number of spatial discretization blocks. The formation dips at an angle of 60° and is modeled in the presence of both a borehole and mud-filtrate invasion. Simulation results are shown for a probing frequency of 220 KHz.

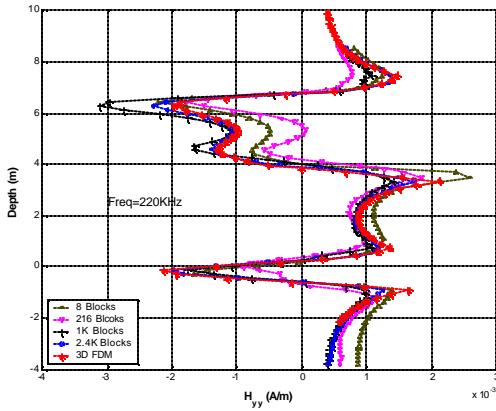


Figure 5. Assessment of the accuracy of the integral equation approximation of H_{yy} (imaginary part) for a given number of spatial discretization blocks. The formation dips at an angle of 60° and is modeled in the presence of both a borehole and mud-filtrate invasion. Simulation results are shown for a probing frequency of 220 KHz.

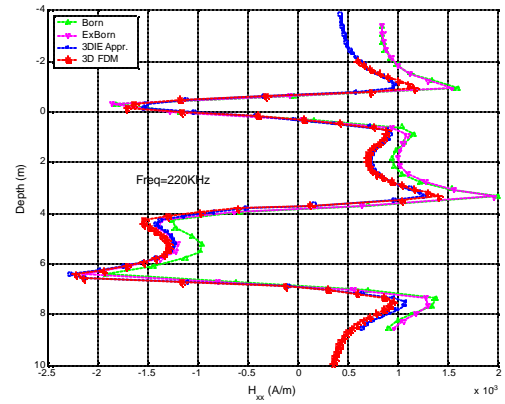


Figure 7. Assessment of the accuracy of the integral equation approximation of H_{xx} (imaginary part) with respect to alternative approximation strategies. The formation dips at an angle of 60° and is modeled in the presence of both a borehole and mud-filtrate invasion. Simulation results are shown for a probing frequency of 220 KHz.

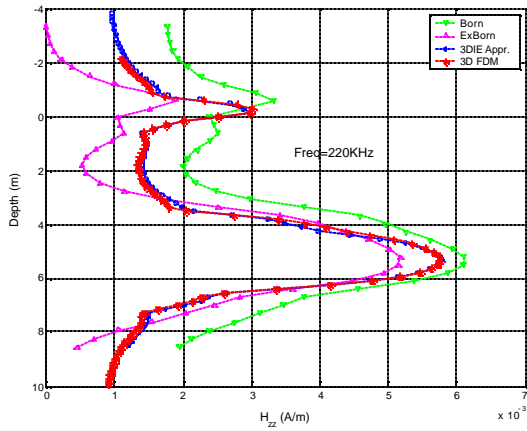


Figure 6. Assessment of the accuracy of the integral equation approximation of H_{zz} (imaginary part) with respect to alternative approximation strategies. The formation dips at an angle of 60° and is modeled in the presence of both a borehole and mud-filtrate invasion. Simulation results are shown for a probing frequency of 220 KHz.

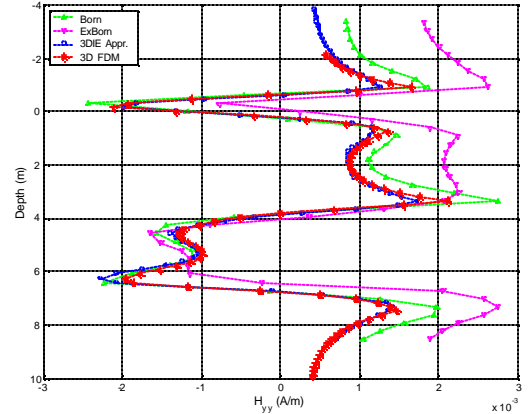


Figure 8. Assessment of the accuracy of the integral equation approximation of H_{yy} (imaginary part) with respect to alternative approximations. The formation dips at an angle of 60° and is modeled in the presence of both a borehole and mud-filtrate invasion. Simulation results are shown for a probing frequency of 220 KHz.

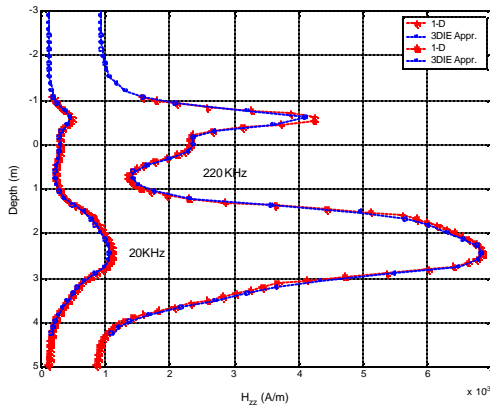


Figure 9. Comparison of the H_{zz} field component (imaginary part) simulated with the new approximation and a 1D code. In both cases, the simulations were performed assuming a 1D formation that exhibits electrical anisotropy. The induction logging tool is assumed to be oriented perpendicular to the formation. Simulation results are shown for probing frequencies of 20 KHz and 220 KHz.

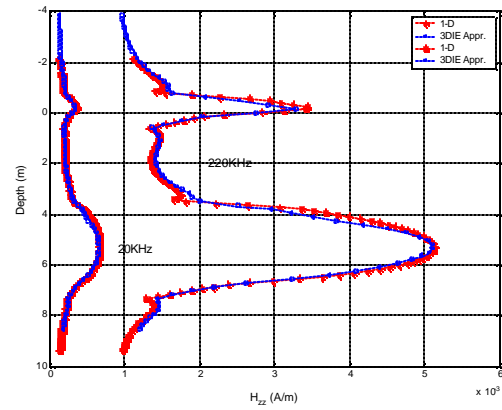


Figure 11. Comparison of the H_{zz} field component (imaginary part) simulated with the new approximation and a 1D code. In both cases, the simulations were performed assuming a 1D formation that exhibits electrical anisotropy and a borehole dipping at an angle of 60° . Simulation results are shown for probing frequencies of 20 KHz and 220 KHz.

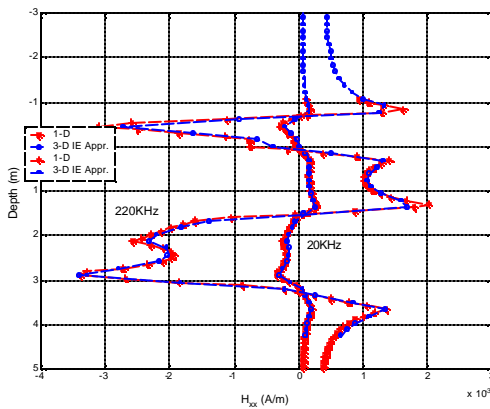


Figure 10. Comparison of the H_{xx} field component (imaginary part) simulated with the new approximation and a 1D code. In both cases, the simulations were performed assuming a 1D formation that exhibits electrical anisotropy. The induction logging tool is assumed to be oriented perpendicular to the formation. Simulation results are shown for probing frequencies of 20 KHz and 220 KHz.

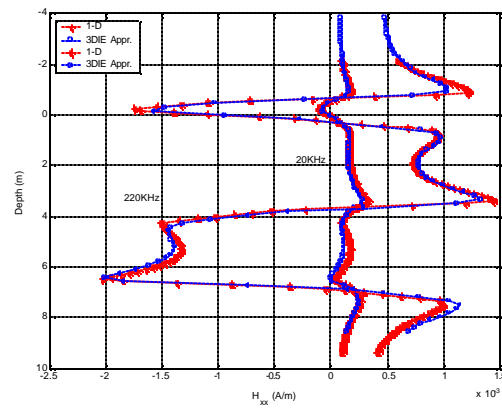


Figure 12. Comparison of the H_{xx} field component (imaginary part) simulated with the new approximation and a 1D code. In both cases, the simulations were performed assuming a 1D formation that exhibits electrical anisotropy and a borehole dipping at an angle of 60° . Simulation results are shown for probing frequencies of 20 KHz and 220 KHz.

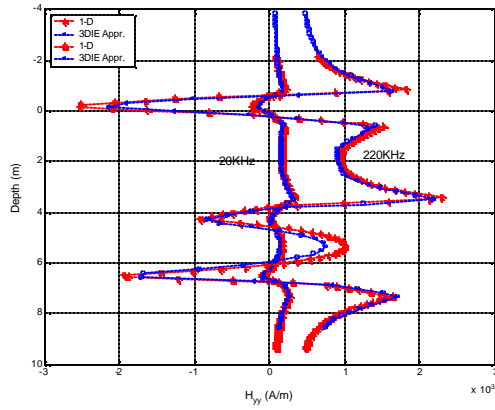


Figure 13. Comparison of the E_{yy} field component (imaginary part) simulated with the new approximation and a 1D code. In both cases, the simulations were performed assuming a 1D formation that exhibits electrical anisotropy and a borehole dipping at an angle of 60° . Simulation results are shown for probing frequencies of 20 KHz and 220 KHz.

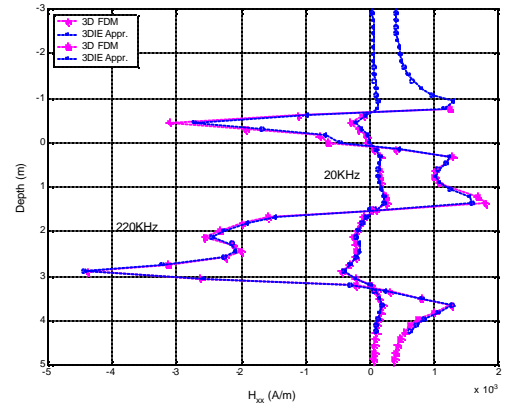


Figure 15. Comparison of the E_{xx} field component (imaginary part) simulated with the new approximation and a 3D-FDM code assuming a 3D formation that includes both a borehole and invasion. The borehole dips at an angle of 0° . Simulation results are shown for the probing frequencies of 20 KHz and 220 KHz.

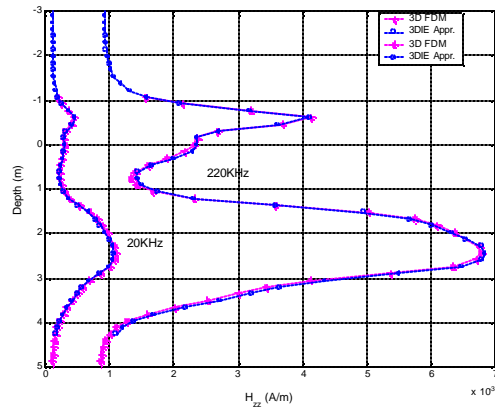


Figure 14. Comparison of the H_{zz} field component (imaginary part) simulated with the new approximation and a 3D-FDM code assuming a 3D formation that includes both a borehole and invasion. The borehole dips at an angle of 0° . Simulation results are shown for the probing frequencies of 20 KHz and 220 KHz.

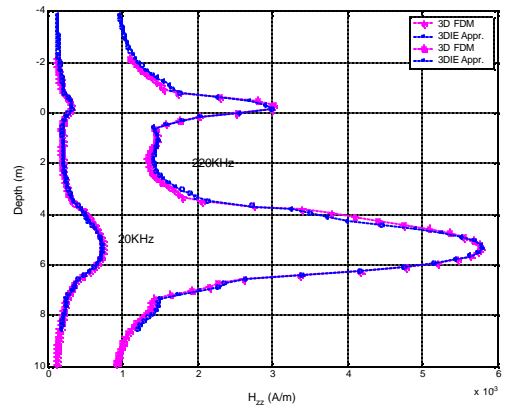


Figure 16. Comparison of the E_{zz} field component (imaginary part) simulated with the new approximation and a 3D-FDM code assuming a 3D formation that includes both a borehole and invasion. The borehole dips at an angle of 60° . Simulation results are shown for the probing frequencies of 20 KHz and 220 KHz.

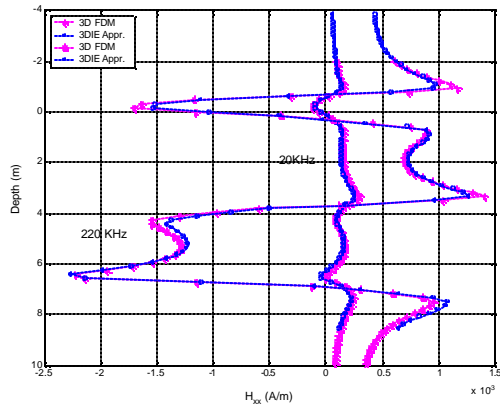


Figure 17. Comparison of the H_{xx} field component (imaginary part) simulated with the new approximation and a 3D-FDM code assuming a 3D formation that includes both a borehole and invasion. The borehole dips at an angle of 60° . Simulation results are shown for the probing frequencies of 20 KHz and 220 KHz.

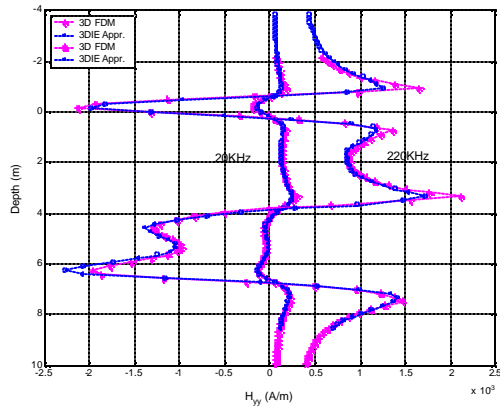


Figure 18. Comparison of the H_{yy} field component (imaginary part) simulated with the new approximation and a 3D-FDM code assuming a 3D formation that includes both a borehole and invasion. The borehole dips at an angle of 60° . Simulation results are shown for the probing frequencies of 20 KHz and 220 KHz.